ELSEVIER

Fluorescence-microscopy-based image analysis for analyte-dependent particle doublet detection in a single-step immunoagglutination assay

Martin Wiklund[a,*], Olof Nord[b], Rikard Gothäll[a], Andrei V. Chernyshev[c], Per-Åke Nygren[b], Hans M. Hertz[a]

[a] *Biomedical and X-Ray Physics, Royal Institute of Technology, AlbaNova University Center, SE-106 91 Stockholm, Sweden*
[b] *Department of Biotechnology, Royal Institute of Technology, AlbaNova University Center, SE-106 91 Stockholm, Sweden*
[c] *Institute of Chemical Kinetics and Combustion, Novosibirsk, Russia*

Abstract

A novel fluorescence-microscopy-based image analysis method for classification of singlet and doublet latex particles is demonstrated and applied to a particle-based immunoagglutination assay for quantification of biomolecules in microliter-volume bulk samples. The image analysis method, verified by flow cytometric agglutination analysis, is based on a pattern recognition algorithm employing Gaussian-base-function fitting which allows robust identification and counting of singlets, doublets, and higher agglomerates of fluorescent microparticles. The immunoagglutination assay is experimentally modeled by a biotin–streptavidin interaction, with the goal of both theoretically and experimentally investigating the performance of a general immunoagglutination-based assay. For this purpose a theoretical model of the initial agglutination kinetics, based on particle diffusion combined with a steric factor determined by the level of specific and nonspecific agglutination, was developed. The theoretical model combined with the experimental data can be used to optimize an agglutination-based assay with regard to sensitivity and dynamic range and to estimate the affinity, receptor surface density, molecular and binding site sizes, and level of nonspecific binding that is present in the assay. The experimental results are in good agreement with the theoretical model, indicating the usefulness of the model for immunoagglutination assay optimization.
© 2004 Elsevier Inc. All rights reserved.

Keywords: Immunoagglutination assay; Image analysis; Aggregation kinetics; Flow cytometry; Nonspecific binding; Microparticles

Antibody-coated latex particles have long been used for immunoagglutination purposes, e.g., in the widely used latex agglutination tests (LATs)[1] [1]. Traditionally, such tests use small particles (10–200 nm) and turbidimetric or nephelometric detection based on light scatter-ing or absorbance [2–4]. Typically, such LAT detection requires formation of large aggregates and has limited sensitivity, even if increased particle collision rate by nonintrusive manipulation methods has improved the situation somewhat [5–8]. More recently, methods monitoring the initial stage of immunoagglutination, the formation of doublet latex microparticles, show promise for improved performance in comparison to LATs. Detection of such doublets has mostly been performed in flow-through systems employing scattered light detection [9–11] or nonintrusive size-selective separation [12,13]. Doublet detection in free solution (bulk) has

---

been performed by the luminescent oxygen channeling immunoassay (LOCI) method [14]. The time-resolved LOCI may detect doublets of sub-μm particles in real time but requires advanced detection equipment and specially sensitized particles. Another approach is to use larger particles (~1 μm) and particle counting detectors based on light scattering measurements combined with flow cells [15–17]. These systems monitor the reduction in counting rate in a flow cell when the particles are agglutinated or the number of unagglutinated particles by light-scattering-based discrimination. Other light scattering instruments based on low-angle light scattering have been used for investigation of particle aggregation [18,19]. Here, the number of particles per cluster has been determined for particles with size smaller than the wavelength. However, for μm-sized particles light scattering evaluation of immunoagglutination remains a problem [9].

Flow cytometry is a powerful and versatile tool primarily for analysis and/or separation of cells. However, by combining analysis of both scattered light and fluorescence, flow cytometry is also useful for sensitive and multiplexed μm-sized particle assays [20,21]. Scanning flow cytometry (SFC) has recently been used for the study of the initial immunoagglutination process [9]. Similar to most particle counting techniques, SFC detection is based on light scattering, but the whole angular dependency of the scattered light from small particle clusters is measured. The SFC technology provides more detailed information about the size and shape of particle clusters than ordinary flow cytometry and can be used for discrimination between singlets, doublets, and triplets of μm-sized particles.

Image analysis in particle-based immunoassays has previously been used for, e.g., intensity measurements of single μm-sized particles [22]. For the immunoagglutination assay, image analysis of particle agglomerates has been employed by measuring the area of the agglomerates [23]. This conventional method is simple but not suitable for detecting the initial stage of agglutination when predominantly singlets and doublets occur.

In this study, we developed a latex agglutination detection scheme based on pattern recognition and classification of singlets and doublets from microscopy images using fluorescent particles. In contrast to previous size-based image analysis algorithms [23], our algorithm is based on shape analysis via fitting of sets of Gaussian base functions. This allows a very high reliability in the classification of singlets, doublets, and multimers, which is verified by control experiments with flow cytometry and manual inspection. In addition, a theoretical model of the initial stage of immunoagglutination is presented. The theoretical model can be used to estimate the level of specific and nonspecific agglutination, in addition to the size and surface density of the biomolecules and their binding sites in the immunoas-
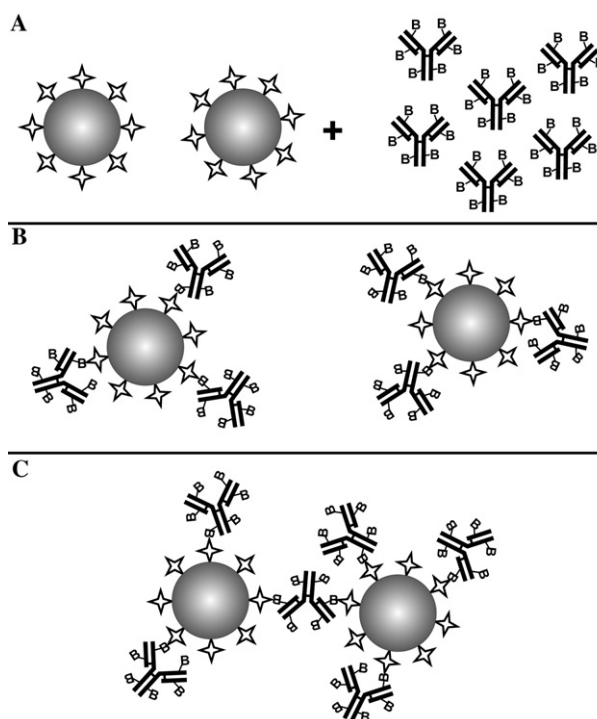

Fig. 1. Immunoagglutination model with a biotinylated IgG (analyte) and streptavidin-coated particles. The three steps illustrate the agglutination mechanism. When the particles are mixed with the analyte (A), the analyte is first bound to the particle surfaces (B), and then an analyte–receptor complex on one particle is agglutinated with a free receptor on another particle (C).

say. By fitting the theoretical model to the experimental data obtained from a model agglutination assay based on the biotin–streptavidin interaction (see Fig. 1), the coupling procedure of the agglutination assay can be optimized, and the performance of a general immunoagglutination assay can be estimated.

Theory

The theory presentation is divided into two parts, the first part describes the image analysis algorithm for identifying and counting singlets and doublets of fluorescent particles from microscopy images, and the second part presents a theoretical model for the kinetics of diffusion-limited immunoagglutination with a steric factor.

Image analysis algorithms

The idea of the image analysis method is to develop an algorithm for classifying singlets and doublets primarily based on the shape of an imaged particle, in contrast to other suggested immunoagglutination image analysis methods, which are based on measuring the area of particle agglomerates [23]. The shape of an

imaged fluorescent particle is close to Gaussian, as shown in Fig. 2. Here, intensity cross sections of 50 imaged 0.9-μm fluorescent particles are plotted (Fig. 2A), and a Gaussian distribution is fitted to the mean cross section of the 50 particles with the background subtracted (solid black curve and dotted gray curve, respectively, in Fig. 2B). Only the shape of the flanks close to the background level differs from the theoretical Gaussian intensity distribution, $I(r)$, which is given by

$$I(r) = I_{max} \cdot \exp(-2(r/r_0)^2), \tag{1}$$

where I_{max} is the maximum intensity at the center of the imaged particle and r_0 is the "Gaussian radius." The image acquisitioning procedure is described in more detail under Materials and methods. Since the intensity cross section is similar to a Gaussian distribution, we have chosen to use a pattern recognition algorithm based on fitting Gaussian base functions to the analyzed regions in an image containing one or several particles. In this way, the image data are transformed to a set of parameters describing the Gaussian distributions, namely position (coordinates x and y), maximum intensity (I_{max}), and radius (r_0). Those parameters can be used for classifying singlets, doublets, and higher agglomerates containing three or more particles.

The analysis is performed on 1600×1200-pixel images typically containing up to 100 particles. The image is first spatially filtered by a low-pass inverse homomorphic filter applied in Fourier space [24]. The purpose of the filter is to suppress high-frequency noise, especially in dark regions of the image, and the result is a reduced background level and a smoothed profile of an imaged particle without distortion of its Gaussian shape.
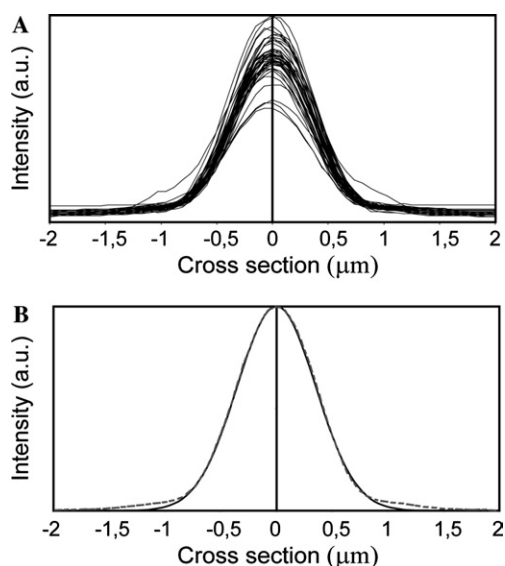
The next step is to find the regions in the image that potentially contain particles. This is performed by transforming the eight-bit gray-scale image by a binary thresholding, resulting in a one-bit image containing continuous areas of white pixels ("islands") surrounded by a black background. Each island defines a delimited area in the image that is a candidate for a singlet, doublet, or a higher agglomerate and is subject for further analysis.

The core algorithm of the image analysis fits a set of Gaussian base functions to each island using the unconstrained nonlinear Nelder–Mead optimization method [25]. The position of the maximum intensity in the island is used as input parameter to the optimization method, in addition to typical values of maximum intensity (I_{max}) and radius (r_0) for a singlet. Basically, the iterative optimization method minimizes the square of the difference between a Gaussian shape and the actual image in the examined delimited region. The final result is a set of up to a maximum of four Gaussian distributions associated with the region, each described by four parameters (x, y, I_{max}, and r_0). The size, place, and number of Gaussian distributions are then used for classifying the examined region into a singlet, doublet, higher agglomerate, or discard.

The classification is based on pattern recognition of the fitted Gaussian distributions to the image. A typical image analysis output is illustrated in Fig. 3. Here, four
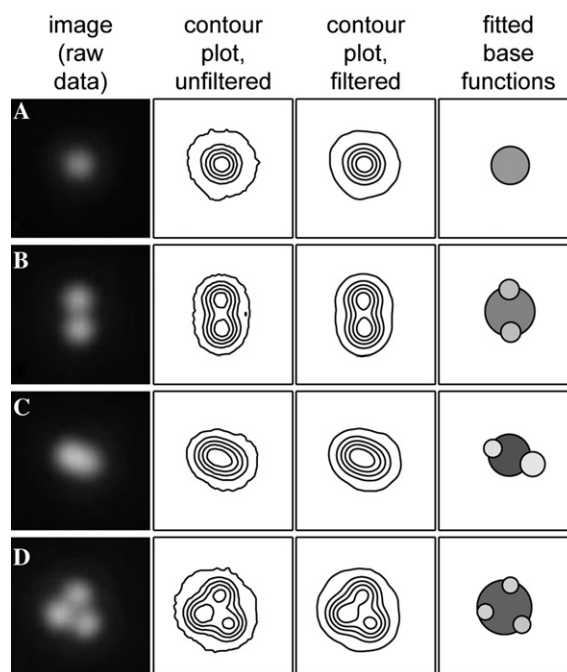

Fig. 3. Raw images, unfiltered contour plots of raw images, filtered contour plots, and fitted Gaussian base functions of a singlet (A), a doublet with nonoverlapping particles (B), a doublet with overlapping particles (C), and a triplet (D). The fitted Gaussian base functions are schematically illustrated by place, size (circles with radius r_0), and maximum intensity (gray scale level proportional I_{max}).

Fig. 2. (A) Measured intensity cross section profiles of the 0.9-μm fluorescent particle used, taken from fluorescence microscopy images of 50 particles. (B) Mean value of all measured profiles (dotted gray curve) and a fitted Gaussian distribution (solid black curve).

different objects are analyzed, a singlet (A), a doublet where both particles are parallel to the image plane (B), the same doublet where the particles are not parallel to the image plane (C), and a triplet where all three particle are parallel to the image plane (d). The first column shows raw image data of the 0.9-μm fluorescent particles. The second and third columns show intensity contour plots of the raw and filtered images, respectively. In the fourth column, the associated Gaussian shapes are illustrated by circles, where the gray level is proportional to I_{max} and the radius is r_0. A singlet is always associated with a single Gaussian distribution and the product $I_{max} \times r_o$ is used for the classification. A doublet is in most cases represented by three distributions, a large distribution positioned at the center of gravity and two satellite distributions marking the positions of each particle. The distance between the satellite distributions is efficiently used for classifying if the particles are in direct contact and the sum of the three products, $\Sigma I_{max,i} \times r_{o,i}$, where $i = 1,2,3$, is used for verification of the two-particle criterion. A more difficult situation is when the doublet is not parallel to the image plane. This case is even hard to classify manually. However, the image analysis algorithm successfully identifies such unresolved doublets as seen in Fig. 3C. Typically, two or three base functions are fitted to the unresolved doublet, and still the sum-product $\Sigma I_{max,i} \times r_{o,i}$ is used for classification. A comparison between Fig. 3B and Fig. 3C reveals that the unresolved doublet has a smaller but more intense center base function and larger but weaker satellite base functions, resulting in small differences between the sum-products $\Sigma I_{max,i} \times r_{o,i}$ of the two imaged doublets. Finally, an agglomerate containing three or more particles can be classified either by having more than three base functions (as in Fig. 3D) or by having a too high sum-product ($\Sigma I_{max,i} \times r_{o,i}$).

Principles of immunoagglutination

The initial stage of the diffusion-limited latex agglutination has been modeled by Surovtsev et al. [9]. The Surovtsev model is based on von Smoluchowski kinetics [26], combined with a steric factor determined by the size and number of binding sites available. In the present paper, the Surovtsev model is extended to also take into account the nonspecific agglutination and the available contact surface between particle clusters. Furthermore, the model is applied to the high-affinity model system used in the experiments, consisting of a streptavidin-coated particle (the solid phase) and a biotinylated antibody (the analyte), by introducing several steric hindrance coefficients.

The basic equations describing the interaction between singlets, doublets, and triplets are given by

$$\frac{dn_1}{dt} = -k(1,1)n_1^2 - k(1,2)n_1n_2 - k(1,3)n_1n_3,$$

$$\frac{dn_2}{dt} = \frac{1}{2}k(1,1)n_1^2 - k(1,2)n_1n_2 - k(2,2)n_2^2 - k(2,3)n_2n_3,$$

and

$$\frac{dn_3}{dt} = k(1,2)n_1n_2 - k(1,3)n_1n_3 - k(2,3)n_2n_3 - k(3,3)n_3^2,$$

$$(2)$$

where n_1, n_2, and n_3 are the time-dependent concentrations of singlets, doublets, and triplets, respectively. The equations describe the very initial stage of agglutination where the concentration of agglomerates containing four particles or more is considered to be negligible. The coefficients $k(i,j)$ are the diffusion-limited agglutination rate constants for the agglutination between a cluster containing i particles and a cluster containing j particles ($i, j = 1, 2, 3$). The rate constants, $k(i,j)$, may be defined as the diffusion-limited rate constants for a small cluster, $k_D(1,1)$, combined with a factor describing the reaction probability, and are given by

$$k(i,j) = \left(\frac{1}{\alpha + ijc_h(i,j)\beta} + 1 \right)^{-1} k_D(1,1), \qquad (3)$$

where

$$k_D(1,1) = \frac{8k_BT}{3\eta}. \qquad (4)$$

The parameters α and β are the probabilities of nonspecific and specific agglutination per one collision between particles, respectively. In our model, α is assumed to be a constant, and β is dependent on the amount of analyte bound to the particle, the geometry of the biotin-binding sites on the particles, and the geometry of the analyte (in our case a biotinylated antibody). The constant $c_h(i,j)$ is the steric hindrance coefficient for collisions between a cluster containing i particles and a cluster containing j particles, since not all surfaces of the clusters are available for contact. For each streptavidin molecule, it is well known that there are four identical biotin-binding sites. The biotinylated antibody was specified by the manufacturer to have on average 6.2 biotin molecules per antibody (see Materials and methods for further details). A specific particle–particle interaction occurs when a binding site on an analyte–receptor complex on one particle collides with a binding site on a free receptor on another particle, as illustrated in Fig. 1. With this knowledge and following [9], the parameter β may be defined as

$$\beta = 5.2b_h \cdot 4s_h N_{1A} N_{1AY} f^{3/2}, \qquad (5)$$

where b_h is the steric hindrance coefficient for the available binding sites on one analyte bound to a particle ($0 < b_h < 1$), and s_h is the corresponding steric hindrance coefficient for the available binding sites on a naked streptavidin molecule anchored on the particle surface ($0 < s_h < 1$). The other parameters in Eqs. (3)–(5) are

the Boltzman constant (k_B), the temperature (T), the viscosity of the medium (η), the amount of free (not occupied) binding sites on the particle (N_{1A}), the amount of analyte–receptor complexes on the particle (N_{1AY}), and the surface fraction occupied by one binding site on the particle (f) given by

$$f = \frac{b^2}{4R^2},\tag{6}$$

where b is the radius of a circular binding site of the receptor (biotin-binding site) and R is the radius of the particle. The cluster-surface steric hindrance coefficients, $c_h(i,j)$, may be determined by calculations of the possible cluster conformations. This has been done by Monte-Carlo simulation of $c_h(i,j)$ for $i+j < 7$ and is presented in Table 1. Basically, the Monte-Carlo simulation averages all possible configurations and orientations of both colliding clusters.

The rate of particle–particle binding is assumed to be much less than the rate of analyte–receptor binding. Therefore, the analyte–receptor binding is treated in equilibrium, and the particle–particle reaction is modeled as an irreversible process. With those assumptions, N_{1A} and N_{1AY} are given by

$$N_{1AY} = \frac{YN_{1A}}{K_D},\tag{7}$$

where K_D is the dissociation constant of the bioaffinity interaction and Y is the concentration of free analyte in the medium given by [9]

$$Y = -\tfrac{1}{2}(I_0 - Y_0 + K_D)$$
$$+ \tfrac{1}{2}\sqrt{(I_0 - Y_0 + K_D)^2 + 4K_DY_0},\tag{8}$$

with $I_0 = n_1(0) \cdot N_{max}$ and $N_{max} = N_{1A} + N_{1AY}$, where I_0 is the initial concentration of receptors, given by the initial concentration of singlets, $n_1(0)$ and the binding capacity of the particle (the amount of receptors on the particle), N_{max}. Furthermore, Y_0 is the initial concentration of free analyte in the medium.

If Eqs. (7 and 8) are combined with Eq. (5), the parameter β can be expressed as a function of the initial concentrations of receptors and analyte, I_0 and Y_0, respectively. Assuming that $K_D \ll Y_0$ and $K_D \ll I_0$ (va-

lid for the experimental biotin–streptavidin agglutination model assay), β may be approximated by

$$\beta = \begin{cases} \gamma \frac{(I_0 - Y_0)Y_0}{I_0^2} & I_0 > Y_0 \\ 0 & I_0 < Y_0, \end{cases}\tag{9}$$

where

$$\gamma = 5.2b_h \cdot 4s_h N_{max}^2 f^{3/2}.\tag{10}$$

Eqs. (9) and (10) express β as the analyte-dependent probability of specific agglutination at each collision event between particles. If the analyte concentration (Y_0) is higher than the receptor concentration (I_0), saturation of analyte–receptor complexes on the particle surfaces will prevent the specific agglutination (often referred to as the "Hook-effect") [27]. In Fig. 4, the normalized β parameter is plotted versus analyte concentration (Y_0) for two different dissociation constants, with typical particle and analyte concentration levels used in the experiments. Curve a illustrates the agglutination probability for the biotin–streptavidin interaction ($K_D = 10^{-14}$ M), and curve b represents a lower-affinity assay, e.g., a good immunoassay ($K_D = 10^{-10}$ M). In case a, the β parameter is approximated with the expression given in Eqs. (9), and (10). This curve drops abruptly to zero when the analyte concentration equals the particle-bound receptor concentration ($Y_0 = I_0$). Furthermore, the curve has a maximum for $Y_{0\,max} = 0.5I_0$, corresponding to a fractional occupancy of analyte on the particles of 50%. It can also be seen in the diagram that the difference between a high-affinity interaction (curve a) and a lower-affinity interaction (curve b) is mainly the curve shape close to the saturation level.
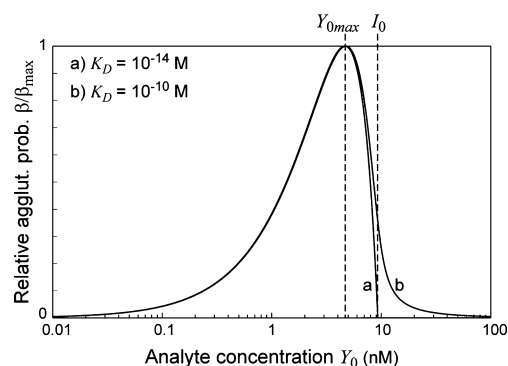

Fig. 4. Calculation of the parameter β, representing the analyte-dependent agglutination probability, plotted versus the analyte concentration Y_0. In the calculation, the particle concentration is 2×10^8 mL^{-1}, and the binding capacity is 2.8×10^4 binding sites per particle. The curve (a) is for $K_D = 10^{-14}$ M (typical for biotin–streptavidin), and the curve (b) is for $K_D = 10^{-10}$ M (typical for a good immunoassay). The curve (a) is given by the approximate value of β in Eq. (9). Here, the analyte concentration at maximum agglutination ($Y_{0\,max}$) is given by $Y_{0\,max} = 0.5I_0$, where I_0 is the initial particle concentration.

Table 1
Monte-Carlo simulation of the cluster–surface steric hindrance coefficient, $c_h(i,j)$, for $i+j < 7$

i	j	$c_h(i,j)$
1	1	1.00 ± 0.01
1	2	0.755 ± 0.006
1	3	0.667 ± 0.006
2	2	0.531 ± 0.005
2	3	0.453 ± 0.003
3	3	0.363 ± 0.002

The detection limit may be defined as the analyte concentration where β is equal to α. For a high-affinity immunoagglutination assay ($K_D \ll Y_0$ and $K_D \ll I_0$) the sensitivity is then given from Eq. (9) as

$$Y_{0\min} = \frac{1}{2} n_1(0) N_{\max} \left(1 - \sqrt{1 - \frac{4\alpha}{\gamma}} \right). \tag{11}$$

Thus, from a sensitivity point of view, the detection limit is basically determined by the concentration of particles in the sample and not by the affinity of the assay, as long as the dissociation constant of the assay is lower than the particle-bound receptor concentration. We may also conclude that, for quantitative measurements, the useful analyte concentration interval (the dynamic range) is delimited to $Y_0 < 0.5 I_0$.

Materials and methods

Materials

Streptavidin-coated fluorescent polystyrene particles (0.90 μm Dragon Green-labeled; 2.8×10^4 FITC–biotin-binding sites per particle) were purchased from Bangs Laboratories (Fishers, IN, USA). Anti-FLAG biotinylated M5 monoclonal antibody (6.2 mole biotin per mole antibody) was used as modeled analyte (Sigma, St. Louis, MO, USA), and anti-FLAG FITC-conjugated M2 monoclonal antibody (Sigma) was used for negative control measurements. Washing/binding (w/b) buffer was phosphate-buffered saline, pH 7.2, with 0.05% Pluronic FL108 NF surfactant from BASF (Mount Olive, NJ, USA).

Sample preparation

The particles were prepared by washing and resuspension in w/b buffer to a concentration of 1×10^{10} mL^{-1}, followed by pulsed tip-sonication to break up initial aggregates of nonspecific-bound particles, and finally diluted with further w/b buffer to the incubation concentration. The antibody was diluted in w/b buffer and put on ice prior to the incubation. Three different particle concentrations were investigated, 2×10^8, 1×10^9, and 1×10^{10} mL^{-1}, and the corresponding antibody concentrations were 0.1, 0.2, 0.4, 0.8, 1.5, and 2.5 nM, 1.5, 5, 12.5, 25, and 50 nM, and 5, 17, 50, 150, 270, and 500 nM, respectively. The corresponding incubation times were 270 min, 30 and 60 min, and 15, 30, 45, and 60 min, respectively. All samples were carried out in duplicates. To 20 μL of calibration sample of diluted antibody, 180 μL of particle reagent was added, resulting in the desired antibody and particle concentrations. The samples were incubated at room temperature (22 °C) with gentle mixing, and the reaction was finally quenched by adding a sample aliquot of 1 to 200 μL w/b buffer.

Apparatus

The image analysis was performed on image sets acquired with an epiilluminated fluorescence microscope (Nikon Eclipse ME600P) equipped with a 100-W mercury lamp and a monochrome CCD camera (SPOT RT Monochrome; Diagnostic Instruments, Sterling Heights, MI, USA). The fluorescence filter set (B-2A; Nikon) was designed for FITC-equivalent fluorophores (excitation between 450 and 490 nm, emission from 530 nm). The objective used was an air immersion CF Plan Apo 100×/0.95 NA with working distance 0.32 mm, and the CCD camera was equipped with a 1600×1200, 7.4-μm-pixel cooled chip (KAI-2000, Kodak).

Comparative flow cytometric analysis was performed on a FACS Vantage SE instrument (BD Biosciences, San Jose, CA, USA). The forward scattered light and the fluorescence from the particles were detected at a rate of approximately 500 events/s and classified into singlets, doublets, and higher agglomerates by analyzing the plotted fluorescence signal versus the forward scattered signal, as shown in Fig. 5. All flow cytometry measurements were performed by measuring the height of the detected intensity peak.
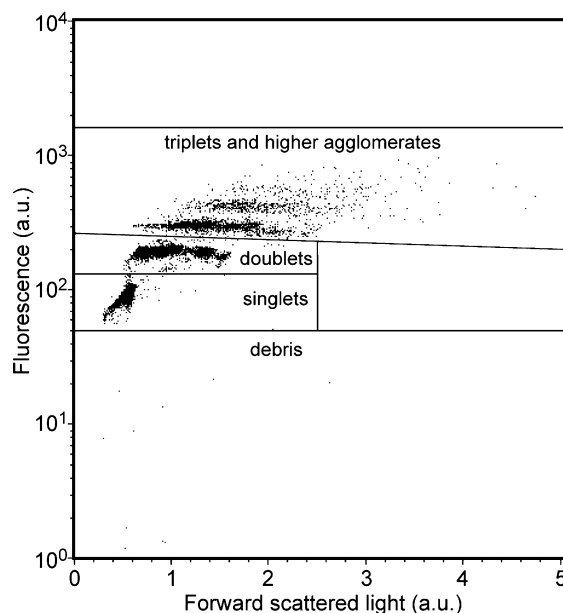

Fig. 5. Typical flow cytometer data, where the height of each detected fluorescence event is plotted versus the height of each detected forward scattering event. The classification into singlets, doublets, and triplets or higher agglomerates (multimers) is indicated. The analyte and particle concentrations are 50 nM and 1×10^{10} mL^{-1}, respectively.

Procedure

For the image analysis, 4 µL of each quenched sample was placed on glass slides with 18×18-mm coverslips on top, resulting in thin sample slices with approximately 10 µm height. The sample volumes were chosen as the smallest possible that fill the whole area under the cover slip. After 10 min all particles were settled close or on the glass slide top surface by gravity. Then, for each sample, at least 100 images were quickly acquired by screening the sample from left to right ($\sim$50 images) and then a second line further down, from right to left (another $\sim$50 images) in a standardized and repeatable manner. The distance between each image was approximately one field-of-view width to avoid overlapping images. This procedure may easily be automated by computer-controlled step motors and camera exposure control.

For the flow cytometric analysis, 200 µL of quenched sample was used and the analysis was performed at several incubation time intervals to acquire data for the theoretical modeling.

Results and discussion

Nonanalyte particle characterization

First, an investigation of the raw data obtained from the two different detection systems (the fluorescence microscope for the image analysis method and the flow cytometer) was performed by comparing the classification parameters for single particles (singlets). In Fig. 6, histograms of these basic singlet classification parameters are
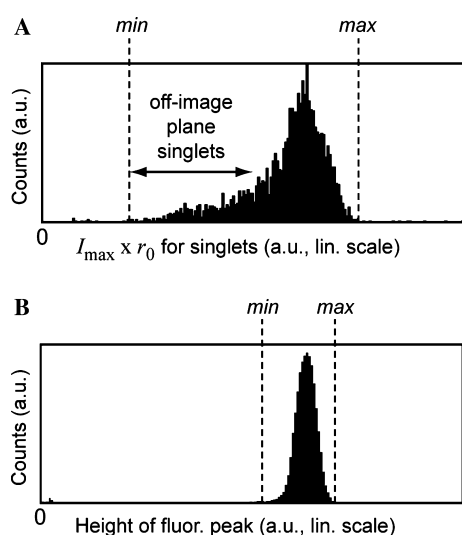
Fig. 6. Comparison of raw data from singlets for the two different methods. (A) Histogram of $I_0 \times r_0$ of $\sim 5 \times 10^3$ singlets resulting from the image analysis method. (B) Histogram of measured height of the fluorescence peak of $\sim 5 \times 10^5$ singlets, resulting from the flow cytometric analysis.

plotted. In Fig. 6A, the value on the x axis is the product $I_{max} \times r_0$ for the fitted base function of $\sim 5 \times 10^3$ singlets, resulting from the image analysis algorithm. In Fig. 6B, the corresponding value on the x axis is the height of the detected fluorescence peak from $\sim 5 \times 10^5$ singlets, resulting from the flow cytometric analysis. Clearly, the distribution is about four times wider for the image analysis method, with a long tail toward lower values from singlets slightly off the image focal plane of the microscope. Furthermore, the highest value of a singlet is about 3× higher than the lowest value (max and min in Fig. 6A, respectively). The diagrams illustrate the reason for not choosing an image analysis algorithm that is based on measuring the total intensity of a particle cluster, since such an algorithm would result in overlapping distributions of singlets and doublets. By instead choosing the shape-based algorithm presented here, off-image-plane particles or nonuniform excitation light distribution over the microscope field-of-view will not reduce the image analysis performance and robustness.

On the other hand, the flow cytometer gives a much more narrow distribution due to the high-performance hydrodynamical focusing of the sample. Thus, the width of the flow cytometric distribution arises from the distribution of the amount of fluorophores in each particle rather than from the instrumental performance. For the flow cytometric analysis, the amount of fluorescence may well be used for the classification between singlets, doublets, and higher agglomerates, as shown in Fig. 5.

Correlation between image analysis and manual inspection

The classification algorithm was calibrated by manual inspection of some images and their corresponding sets of fitted base functions. The camera exposure time and excitation light intensity were adjusted to allow fast image acquisitioning ($\sim$100 ms per image) but still utilizing the whole dynamic range of the camera. However, if the excitation light intensity was too high, bleaching of the particle leading to even wider intensity distributions occurred. This was avoided by a quick and standardized acquisition procedure, with minimized light exposure time prior to each image taken. After proper adjustment of the acquisition procedure, the parameter intervals for I_{max} and r_0 for each set of fitted base functions (one, two, three, or four base functions) were calibrated.

Several sets of images with various amounts of singlets and doublets were acquired. The particles were classified by the image analysis algorithm into singlets, doublets, and multimers containing three particles or more. In all comparisons, there were no noticeable differences between the results from the image analysis method and those from the manual classification. However, the subjective manual inspection should not be considered a good reference for verification of the image analysis method. In

many cases, it is difficult to perform a reliable manual classification. This is illustrated in Fig. 3c, where a doublet is imaged when the two particles are heavily overlapping. The raw images in Figs. 3b and c are taken of a moving doublet at two different positions, and evidently it is much easier to manually classify the doublet in position b than in position c. However, after several similar experiments on the classification performance for differently oriented doublets, the image analysis method has proved to be more reliable than a manual classification.

Correlation between image analysis and flow cytometry

Similar experiments were performed to correlate the image analysis results to the flow cytometric results. In Fig. 7, the fractions of singlets, doublets, and higher agglomerates are plotted for different samples measured with both methods. The calculated correlation coefficients are 0.93 (singlets), 0.85 (doublets), and 0.93 (multimers). There is a large difference in counted events for the two methods; the flow cytometer counts 100 times more events. Still, each data point for the image analysis method represents ∼5000 events, which is sufficient for reliable statistics. In flow cytometric analysis, there might be a risk that shear forces from the highly pressurized flow will break a doublet apart. Furthermore, there is also a risk that a doublet passes though the detection point with the two particles oriented parallel with the laser beam. Since the flow cytometer detection is performed by measuring the height of an intensity peak for each counted event, a false singlet may then be counted. These could be the reasons for the small difference between image analysis and flow cytometry classification. However, there is no significant difference between the results from the two different methods, since all correlation coefficients are of the order of 0.9.

Agglutination dependency on particle and analyte concentrations

Different particle concentrations and incubation times were used to investigate the initial analyte-dependent
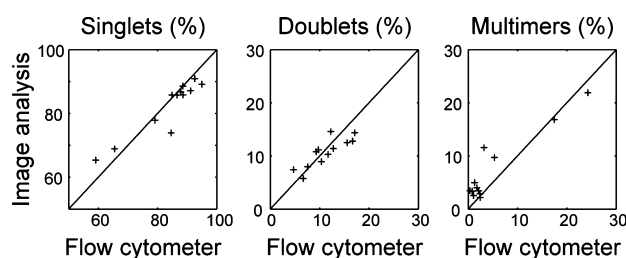

Fig. 7. Correlation between the image analysis results and the flow cytometric analysis results. The corresponding fractions of singlets, doublets, and multimers (triplets and higher agglomerates) are plotted and compared with the 45° straight line. The correlation coefficients are 0.93 (singlets), 0.85 (doublets), and 0.93 (multimers).

agglutination process. The preparations of the particle reagents and the samples of antibodies modeling the immunoassay analyte are described under Materials and methods. Before the antibody samples were mixed with the particle reagent, the singlet and doublet levels were measured to assure that the number of initial singlets ($n_1(0)$) was maximized. The pulsed tip-sonication (15 pulses during 30 s) was found to be more efficient than a standard sonicator bath. The initial amount of singlets was 97–99% at the start of the incubation. In Fig. 8A, the response curves for a high and a low particle concentration ($n_1(0) = 2 \times 10^8$ and 1×10^{10} mL^{-1}) are plotted to demonstrate the analyte-dependent agglutination correlation between image analysis and flow cytometry. The curves show the expected dependency on the antibody concentration according to Eq. (9) and Fig. 4. From the background level of nonspecific agglomerates, the agglutination increases within an interval up to a maximum point, after which the amount of singlets increases and the amount of doublets decreases due to saturation of receptor–analyte complexes on the particle surfaces. From Fig. 8A, it is clear that the level of agglutination is highest for the high particle concentration (1×10^{10} mL^{-1}), which also generates the highest amount of larger agglomerates. However, for the low particle concentration (2×10^8 mL^{-1}) the generation of triplets and higher agglomerates is much lower, resulting in a steeper slope of the doublet curve. In addition, the slope of the doublet curve is steeper for the image analysis method than for the flow cytometry method for the lowest particle concentration. To thoroughly investigate the sensitivity, dynamic range, and performance of the biotin–streptavidin interaction agglutination assay, flow cytometry measurements were performed for two different particle concentrations ($n_1(0) = 1 \times 10^9$ and 1×10^{10} mL^{-1}) and at several different incubation times also including negative control experiments with an unbiotinylated antibody (see Figs. 8B and C). The reason for choosing only flow cytometry analysis for these measurements is the high throughput and level of automation that this instrument offers, making dynamic incubation investigations possible. The concentration of analyte at maximum agglutination level, Y_{0max}, is marked for each particle concentration, $n_1(0)$, in the diagrams in Fig. 8. The ratio of each Y_{0max} to its corresponding particle concentration ($n_1(0)$) may be used to estimate the maximum number of analyte–receptor complexes that can be formed on the particle surface. The four values of Y_{0max} marked in Fig. 8 result in a mean ratio ($Y_{0max}/n_1(0)$) of approximately 1.5×10^{-8} nM × mL. Eq. (9) reveals that the maximum agglutination level is obtained for $Y_{0max} = 0.5 \times I_0 = 0.5 \times n_1(0) \times N_{max}$. Thus, we obtain the binding capacity of the biotinylated antibody as $N_{max} = 2 \times Y_{0max}/n_1(0) = 2 \times 1.5 \times 10^{-8} \times 10^{-9} \times 10^{-3} \times 6 \times 10^{23} = 1.8 \times 10^4$. This value is roughly three times higher than the total number of streptavidin molecules
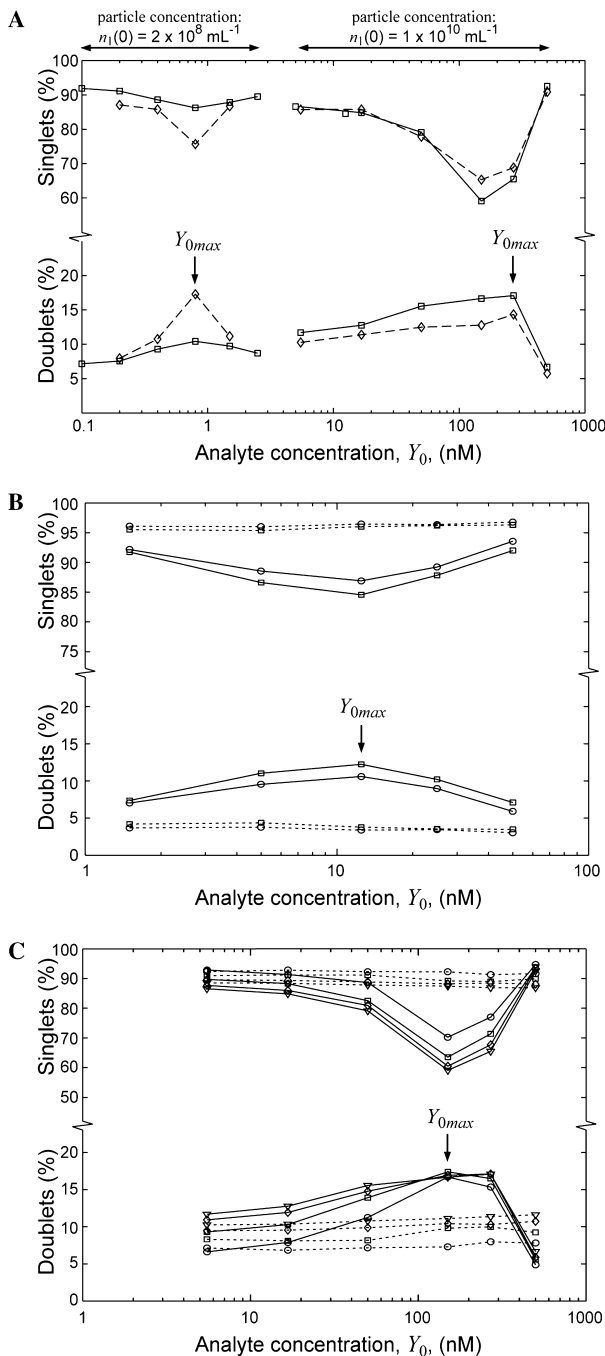
Fig. 8. Dependence of agglutination on the analyte concentration (Y_0) and the particle concentration ($n_1(0)$). (A) Flow cytometric results (solid lines) and image analysis results (dashed lines) for low particle concentration ($n_1(0) = 2 \times 10^8$ mL^{-1}) and high particle concentration ($n_1(0) = 1 \times 10^{10}$ mL^{-1}), after incubation for 270 and 60 min, respectively. (B) Time-dependent agglutination of biotinylated antibody (solid lines) and unbiotinylated antibody (dotted lines) at the particle concentration $n_1(0) = 1 \times 10^9$ mL$^{/1}$ after 30 (○) and 60 (□) min, of incubation, measured with the flow cytometer. (C) Time-dependent agglutination of biotinylated antibody (solid lines) and unbiotinylated antibody (dotted lines) at the particle concentration $n_1(0) = 1 \times 10^{10}$ mL^{-1} after 15 (○), 30 (□), 45 (♦), and 60 (▽) min of incubation, measured with the flow cytometer.

anchored on the particle surface (6×10^3), calculated from the binding capacity of FITC–biotin to the particles (2.8×10^4), specified by the manufacturer. Thus, the results indicate that each streptavidin molecule on the particle surface can bind three molecules of biotinylated antibody. The size of a streptavidin molecule ($\sim$5 nm) [28] is half the size of the antibody ($\sim$10 nm) [29] and the average distance between the streptavidin molecules is $\sim$20 nm. Therefore, there may be enough space to bind three biotinylated antibody molecules taking into account that streptavidin is anchored to the particle surface (i.e., the fourth side is unavailable for binding of the antibody due to steric hindrance).

Treatment of the experimental results by the theoretical model

The experimental data from all measurements in Fig. 8 were treated by the model of the initial stage of immunoagglutination presented under Theory. The important parameters in the model are the probabilities for non-specific and specific binding at each collision between particles (α and β), respectively. We have assumed that the parameter α is a constant and not dependent on the analyte concentration. This assumption is valid within the precision of the experiments and has been confirmed by negative control experiments using a non-biotinylated antibody (anti-FLAG M2 FITC-conjugated monoclonal antibody) (see Figs. 8B and C). The inputs for the fitting are the experimentally determined $n_1(t)$, $n_2(t)$, and $n_3(t)$ (cf. Eq. (2)) for the three different initial particle concentrations ($n_1(0)$) and for the different incubation times (t). The outputs for each measurement series are the parameters α and γ. The parameter γ can be regarded a weight of β, also taking into account the analyte concentration (cf. Eq. (9)). The results of the fitting are presented in Table 2. The ratio of the specific to the nonspecific agglutination probability in our experiments is $\gamma/\alpha \approx 20$, with the trend of increasing ratio with increasing particle concentration. From the parameter γ it is possible to estimate the size of the binding site. For example, if we assume that $s_h \sim 3/4$, $b_h \sim 1/2$, and $N_{\max} \sim 1.8 \times 10^4$, Eqs. (6 and 10) give the radius of the binding site $b \approx 0.2$ nm. Therefore, the estimated size (diameter) of the binding site is approximately 0.4 nm. This value is rather close to the size of the biotin molecule.[2]

Prediction of the sensitivity

Good agreement of the theoretical model with the experimental data allows us of the model to predict

Table 2
Fitting of the nonspecific (α) and specific (γ) agglutination probabilities to the experimental data ($n_1(t)$, $n_2(t)$, and $n_3(t)$)

Analyte	$n_1(0)$ [mL^{-1}]	t [min]	Y_0 [nM]	α (nonspecific)	γ (specific)	γ/α
M5	2×10^8	0, 270	0.1–2.5	$(2.0 \pm 0.4) \times 10^{-3}$	$(2.5 \pm 0.4) \times 10^{-2}$	13
M5	1×10^9	0, 30, 60	1.5–50	$(1.7 \pm 0.3) \times 10^{-3}$	$(3.9 \pm 0.3) \times 10^{-2}$	23
M5	1×10^{10}	0, 15, 30, 45, 60	5–500	$(1.1 \pm 0.2) \times 10^{-3}$	$(3.2 \pm 0.3) \times 10^{-2}$	29
M2[a]	1×10^9	0, 30, 60	1.5–50	$(1.33 \pm 0.05) \times 10^{-3}$	—	—
M2[a]	1×10^{10}	0, 15, 30, 45, 60	5–500	$(0.64 \pm 0.01) \times 10^{-3}$	—	—

[a] Negative control.

the detection limit of the immunoagglutination assay modeled by the biotin–streptavidin system. The theoretical detection limit is defined in Eq. (11), and is dependent on the initial particle concentration, $n_1(0)$, and the ratio of the specific to the nonspecific agglutination probability, γ/α. For example, the detection limit is of the order of 100 pM for a particle concentration $n_1(0) = 10^8$ mL^{-1}, a binding capacity $N_{max} = 1.8 \times 10^4$, and a γ/α ratio between 20 and 30. This limit is approximately half the observed experimental detection limit in Fig. 8A. Eq. (11) illustrates that a higher sensitivity may be achieved by either lowering $n_1(0)$, lowering N_{max}, or increasing the γ/α ratio. The detection limit is scaled linear to $n_1(0)$ and N_{max}, but a very low $n_1(0)$ also results in excessively long incubation times. Furthermore, a lower N_{max} will decrease the absolute values of α and γ and, therefore, β, which also results in longer incubation times. In addition, it may be assumed that a lower binding capacity of the particles (i.e., larger mean distances between each receptor on the particle surface) will result in a higher level of nonspecific agglutination. For example, larger hydrophobic areas of uncoated latex typically increase the problem with nonspecific binding. However, Eq. (11) also reveals that the sensitivity is increasing very slowly with the γ/α ratio, indicating that the most important parameters determining the sensitivity are the particle concentration and the binding capacity of the particles. Finally, it should be mentioned that the dynamic range of the immunoagglutination assay for quantitative measurements is given by $Y_{0min} < Y_0 < 0.5 \times I_0$, where Y_{0min} is given by Eq. (11). For the biotin–streptavidin system the dynamic range is typically two orders of magnitude. However, if a lower-affinity system is employed, e.g., an immunoassay where the dissociation constant is of the order of the receptor and analyte concentrations, the change in sensitivity is small, but the dynamic range is increased.

Conclusions

We have developed a novel detection method for counting and classifying singlets and doublets of immunoagglutinated µm-sized fluorescent particles by pattern-recognition-based image analysis on a fluorescence-microscopy platform. The method identifies singlets and doublets in bulk samples by screening large numbers of images from glass slide samples. Despite nonoptimized imaging conditions, e.g., nonuniform excitation light distribution and off-image-plane particles, the image analysis method is robust and reliable in the classification and is even better than counting by manual inspection. In addition, small sample volumes are needed (few µL), and the method may well be automated and implemented in small scale. We also conclude that the method is equally good as flow-cytometry-based agglutination analysis, even if the present levels of automation and throughput are not yet comparable. The best performance of the image analysis immunoagglutination method is for low particle concentration generating small agglomerates, mainly doublets. Since the image analysis method is tailor-made for detecting doublets, the method has potential to detect lower analyte concentrations in comparison to the traditional latex agglutination tests. At higher analyte and particle concentrations, the doublet level is quickly emptied, and larger agglomerates are formed, making the method less suitable. Furthermore, a theoretical model describing the agglutination dependence on the level of nonspecific binding, assay affinity, and molecular geometries was developed. By fitting the model to experimental data, important feedback that can be used for efficient optimization of the agglutination performance, e.g., the sensitivity, dynamic range, and incubation time, is given. Furthermore, this work has implications for the proposed methods for ultrasensitive analysis via doublet detection and/or doublet enrichment by ultrasonic trap-enhanced capillary electrophoresis [30]. This method shows promise for very high sensitivity from their physical properties while nonspecific agglutination (NSA) and incubation time might well be the limiting factors.

Future improvement of our suggested image analysis method is to suppress the NSA and to investigate other particle-enhanced immunoassays with dissociation constants lower than those of the biotin–streptavidin interaction. Plenty of work has been done to investigate the factors that contribute to the colloidal stability of the particle suspension and the rate of NSA [31–33]. The NSA has to be optimized for each type of immunoassay used. Other possibilities for improvement are to

use magnetic or unsymmetrically coated particles [34]. Magnetic particles could be used to quickly immobilize the particles on the bottom surface of the glass slide and to put both particles in a doublet in the image plane of the microscope. Unsymmetrically coated particles could be used to minimize the generation of triplets and higher agglomerates, making the doublet response curve even steeper. Furthermore, higher specificity could also be obtained by the use of monoclonal antibodies directed against two different epitopes on one and the same target protein [35]. By labeling the type-1-antibody-coated particle in one color and the type-2-antibody-coated particle in another color, only multicolored doublets are counted. Multiplexing is also possible in the same approach as that in the flow-cytometric-based suspension array technology [20]. However, one of the most important advantages of the image analysis method for future improvements is the compatibility to existing high-throughput screening platforms and to the lab-on-chip format.

Acknowledgment

References

[1] D.J. Newman, H. Henneberry, C.P. Price, Particle enhanced light scattering immunoassay, Ann. Clin. Biochem. 29 (Pt 1) (1992) 22–42.

[2] O. Deegan, K. Walshe, K. Kavanagh, S. Doyle, Quantitative detection of C-reactive protein using phosphocholine-labelled enzyme or microspheres, Anal. Biochem. 312 (2003) 175–181.

[3] W.H. Kapmeyer, H.E. Pauly, P. Tuengler, Automated nephelometric immunoassays with novel shell core particles, J. Clin. Lab. Anal. 2 (1988) 76–83.

[4] W.J. Litchfield, A.R. Craig, W.A. Frey, C.C. Leflar, C.E. Looney, M.A. Luddy, Novel shell/core particles for automated turbidimetric immunoassays, Clin. Chem. 30 (1984) 1489–1493.

[5] M.I. Song, K. Iwata, M. Yamada, K. Yokoyama, T. Takeuchi, E. Tamiya, I. Karube, Multisample analysis using an array of microreactors for an alternating-current field-enhanced latex immunoassay, Anal. Chem. 66 (1994) 778–781.

[6] Z. Sun, S. Xu, G. Dai, Y. Li, L. Lou, Q. Liu, R. Zhu, A microscopic approach to studying colloidal stability, J. Chem. Phys. 119 (2003) 2399–2405.

[7] M.A. Sobanski, R.W. Ellis, J.G. Hastings, Rotavirus detection using ultrasound enhanced latex agglutination and turbidimetry, J. Immunoassay 21 (2000) 315–325.

[8] S. Bhaskar, J.N. Banavaliker, K. Bhardwaj, P. Upadhyay, A novel ultrasound-enhanced latex agglutination test for the detection of antibodies against Mycobacterium tuberculosis in serum, J. Immunol. Methods 262 (2002) 181–186.

[9] I.V. Surovtsev, M.A. Yurkin, A.N. Shvalov, V.M. Nekrasov, G.F. Sivolobov, A.A. Grazhdantseva, V.P. Maltsev, A.V. Chernyshev, Kinetics of the initial stage of immunoagglutionation studied with the scanning flow cytometer, Colloid Surface B 32 (2003) 245–255.

[10] N. Pamme, R. Koyama, A. Manz, Counting and sizing of particles and particle agglomerates in a microfluidic device using laser light scattering: application to a particle-enhanced immunoassay, Lab. Chip 3 (2003) 187–192.

[11] Z. Rosenzweig, E.S. Yeung, Laser-based particle-counting microimmunoassay for the analysis of single human erythrocytes, Anal. Chem. 66 (1994) 1771–1776.

[12] T. Hatano, T. Kaneta, T. Imasaka, Application of optical chromatography to immunoassay, Anal. Chem. 69 (1997) 2711–2715.

[13] M. Wiklund, S. Nilsson, H.M. Hertz, Ultrasonic trapping in capillaries for trace-amount biomedical analysis, J. Appl. Phys. 90 (2001) 421–426.

[14] E.F. Ullman, H. Kirakossian, S. Singh, Z.P. Wu, B.R. Irvin, J.S. Pease, A.C. Switchenko, J.D. Irvine, A. Dafforn, C.N. Skold, et al., Luminescent oxygen channeling immunoassay: measurement of particle binding kinetics by chemiluminescence, Proc. Natl. Acad. Sci. USA 91 (1994) 5426–5430.

[15] C.L. Cambiaso, A.E. Leek, F. De Steenwinkel, J. Billen, P.L. Masson, Particle counting immunoassay (PACIA). I.A general method for the determination of antibodies, antigens, and haptens, J. Immunol. Methods 18 (1977) 33–44.

[16] P.L. Masson, Particle counting immunoassay—an overview, J. Pharmaceut. Biomed. 5 (1987) 113–117.

[17] L.M. Galanti, J. Dell'Omo, B. Wanet, J.L. Guarin, J. Jamart, M.G. Garrino, P.L. Masson, C.L. Cambiaso, Particle counting assay for anti-toxoplasma IgG antibodies. Comparison with four automated commercial enzyme-linked immunoassays, J. Immunol. Methods 207 (1997) 195–201.

[18] M.S. Bowen, M.L. Broide, R.J. Cohen, Determination of cluster size distributions using an optical pulse particle-size analyzer, J. Colloid Interf. Sci. 105 (1985) 605–616.

[19] M.L. Broide, R.J. Cohen, Measurements of cluster-size distributions arising in salt-induced aggregation of polystyrene microspheres, J. Colloid Interf. Sci. 153 (1992) 493–508.

[20] J.P. Nolan, L.A. Sklar, Suspension array technology: evolution of the flat-array paradigm, Trends Biotechnol. 20 (2002) 9–12.

[21] X. Song, J. Shi, B. Swanson, Flow cytometry-based biosensor for detection of multivalent proteins, Anal. Biochem. 284 (2000) 35–41.

[22] F. Szurdoki, K.L. Michael, D.R. Walt, A duplexed microsphere-based fluorescent immunoassay, Anal. Biochem. 291 (2001) 219–228.

[23] N.E. Thomas, W.T. Coakley, Measurement of antigen concentration by an ultrasound-enhanced latex immunoagglutination assay, Ultrasound Med. Biol. 22 (1996) 1277–1284.

[24] R.C. Gonzalez, R.E. Woods, Digital Image Processing, Addison-Wesley, San Francisco, 1992.

[25] A. Quarteroni, R. Sacco, F. Saleri, Numerical Mathematics, Springer, NY, 2000.

[26] M.Z. von Smoluchowski, Versuch einer mathematischen theorie der koagulationskinetik kolloiderlösungen, Phys. Chem. 92 (1917) 129–168.

[27] J. Frengen, K. Nustad, R. Schmid, T. Lindmo, A sequential binding assay with a working range extending beyond seven orders of magnitude, J. Immunol. Methods 178 (1995) 131–140.

[28] W.A. Hendrickson, A. Pahler, J.L. Smith, Y. Satow, E.A. Merritt, R.P. Phizackerley, Crystal structure of core streptavidin determined from multiwavelength anomalous diffraction of synchrotron radiation, Proc. Natl. Acad. Sci. USA 86 (1989) 2190–2194.

[29] R.C. Valentine, N.M. Green, Electron microscopy of an antibody-hapten complex, J. Mol. Biol. 27 (1967) 615–617.

[30] M. Wiklund, P. Spegel, S. Nilsson, H.M. Hertz, Ultrasonic-trap-enhanced selectivity in capillary electrophoresis, Ultrasonics 41 (2003) 329–333.

[31] S. Perez-Amodio, P. Holownia, C.L. Davey, C.P. Price, Effects of the ionic environment, charge, and particle surface chemistry for

enhancing a latex homogeneous immunoassay of C-reactive protein, Anal. Chem. 73 (2001) 3417–3425.

[32] P. Holownia, S. Perez-Amodio, C.P. Price, Effect of poly(ethylene glycol), tetramethylammonium hydroxide, and other surfactants on enhancing performance in a latex particle immunoassay of C-reactive protein, Anal. Chem. 73 (2001) 3426–3431.

[33] J.Y. Yoon, K.H. Kim, S.W. Choi, J.H. Kim, W.S. Kim, Effects of surface characteristics on non-specific agglutination in latex immunoagglutination antibody assay, Colloid Surface B 27 (2003) 3–9.

[34] K. Fujimoto, K. Nakahama, M. Shidara, H. Kawaguchi, Preparation of unsymmetrical microspheres at the interfaces, Langmuir 15 (1999) 4630–4635.

[35] H. Nilsson, M. Wiklund, T. Johansson, H.M. Hertz, S. Nilsson, Microparticles for selective protein determination in capillary electrophoresis, Electrophoresis 22 (2001) 2384–2390.